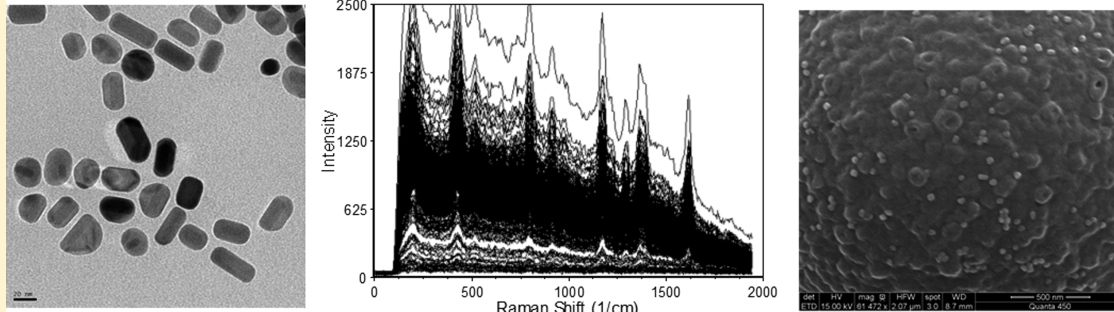


Optimization of SERS Tag Intensity, Binding Footprint, and Emittance

John P. Nolan,*† Erika Duggan, and Danilo Condello

La Jolla Bioengineering Institute Suite 210 3535 General Atomics Court San Diego, California 92121, United States

Supporting Information



ABSTRACT: Nanoparticle surface enhanced Raman scattering (SERS) tags have attracted interest as labels for use in a variety of applications, including biomolecular assays. An obstacle to progress in this area is a lack of standardized approaches to compare the brightness of different SERS tags within and between laboratories. Here we present an approach based on binding of SERS tags to beads with known binding capacities that allows evaluation of the average intensity, the relative binding footprint of particles in a SERS tag preparation, and the size-normalized intensity or emittance. We tested this on four different SERS tag compositions and show that aggregated gold nanorods produce SERS tags that are 2–4 times brighter than relatively more monodisperse nanorods, but that the aggregated nanorods are also correspondingly larger, which may negate the intensity if steric hindrance limits the number of tags bound to a target. By contrast, SERS tags prepared from smaller gold nanorods coated with a silver shell produce SERS tags that are 2–3 times brighter, on a size-normalized basis, than the Au nanorod-based tags, resulting in labels with improved performance in SERS-based image and flow cytometry assays. SERS tags based on red-resonant Ag plates showed similarly bright signals and small footprint. This approach to evaluating SERS tag brightness is general, uses readily available reagents and instruments, and should be suitable for interlab comparisons of SERS tag brightness.

Surface enhanced Raman scattering (SERS) is a phenomenon with significant potential in analytical and bioanalytical chemistry.^{1–3} This potential stems from the molecular information contained in Raman scattering spectra and the great increases in Raman scattering intensity that result from localized electric fields in certain nanostructures. However, these signal enhancements and specificity have proven difficult to harness in a general way, and the development of robust SERS-based analytical methods is very much a work in progress.

One implementation of the SERS phenomenon involves the fabrication of nanoparticle-based SERS labels or tags for antibodies or other targeting molecules.^{4–7} SERS signals can be as bright as fluorescence with better photostability, and the narrow spectral features have great potential for multiplexing. In their most general form, SERS tags are composed of a plasmonic nanoparticle that generates a strong electric field upon illumination with an appropriate light source, a Raman-active compound that confers a distinct spectral signature, and a stabilizing coating that also provides a surface for functionalization with a molecular recognition element such as an antibody. Silica-coated gold nanospheres can be viewed as the prototypical SERS tag,^{8,9} and these have been characterized extensively in terms of fundamental properties^{10–12} and

practical applications.^{13–15} The hot spots of high E-field intensity that form at the interface of nanosphere dimers and trimers have been exploited to make SERS tags with significantly increased intensity.¹² Gold nanorods have also been extensively characterized as plasmonic nanoparticles^{16–21} and can produce bright SERS tags^{22,23} because of the high electric fields that can occur at the ends of the rods. Mixed metal core–shell structures composed of, for example, gold and silver can also result in bright SERS tags.^{24–27} For any SERS tag, the brightness of individual tags is obviously a major determinant of the performance of an assay that employs them, but there are few standard measures of SERS tag brightness.

SERS tags have been used as labels in applications ranging from immunoassays to molecular analysis of cells and tissues;^{6,28–35} however, these demonstrations have not matured into widely used or useful methods. At least one of the reasons for this is a lack of standardized methods for characterization of the SERS tag reagents that would allow, for example, the analysis of the dependence of an assay's analytical performance

Received: January 20, 2014

Revised: May 5, 2014

Published: June 3, 2014

on the properties (intensity, size) of the SERS tag. The enhancement factor is an often-cited property of a SERS tag but, as a relative measure of the effect of the nanoparticle on the scattering intensity of an adsorbed compound, this value is of limited use in predicting assay performance. The intensity of a bulk suspension of SERS tag can be a useful measure, but uncertainties about SERS tag concentrations, size heterogeneity, and a lack of widely accepted external intensity standards for calibrating intensity present significant hurdles for this approach. Single particle analysis methods that provide correlated size and intensity information on many individual nanoparticles in a population would be ideal, but these approaches can be slow, labor intensive, and involve complex and often custom instrumentation that is not suitable for widespread use.

Our lab is interested in using SERS tags as labels for antibodies in single cell analysis. We know that the number of antigens per cell might range from a few thousand to several hundred thousand and that optimizing the discrimination of cells expressing low levels of antigen from those expressing none is essential for many applications. It is reasonable to expect that a more intense SERS tag will perform better at this task, but we can also anticipate that larger sized SERS tags might lead to undesired effects like less efficient binding and steric hindrance on the surface of the cell, so it is important to consider both of these features in optimizing SERS tags for this purpose.

Microspheres have many uses in the calibration of analytical measurements, especially in flow cytometry where polymer beads play roles as intensity calibration and reference standards,^{36–40} particle counting standards,⁴¹ and in reagent characterization.^{35,42–44} We created calibrated capture beads bearing avidin and, using flow cytometry, we are able to characterize the effective size-normalized intensity, or emittance, of biotinylated SERS tags in a manner that helps predict the performance of those tags in an assay. We applied this approach to four different SERS tag compositions and compare these results with those obtained by TEM, SEM, and nanoparticle tracking analysis (NTA). We then prepared antibody conjugates of similar tags to stain cell surface receptors for flow cytometry and found that tag performance in this application correlated with the emittance estimated by our calibration approach. This approach is general and can be applied to any SERS tag formulation, allowing objective comparison of the emittance of different SERS tag compositions and facilitating rational optimization of the performance of SERS tag-based assays.

RESULTS AND DISCUSSION

Our SERS calibration approach is based on surfaces with a known number of SERS tag binding sites. Here, these are polymer microspheres functionalized with different amounts of neutravidin that can be quantified using conventional fluorescence flow cytometry. To create microspheres with defined numbers of binding sites and surface densities, we mixed neutravidin with BSA in different ratios and coupled these to microspheres. The microspheres were fluorescently encoded with different intensities of a green fluorochrome and by different diameters so that they can be identified in a mixture. Staining this multiplexed bead set allows us to assess capture protein capacity and density simultaneously in one tube. As presented in Figure 1A, 3.5- μm -diameter beads bearing different amounts of capture protein could be identified by their

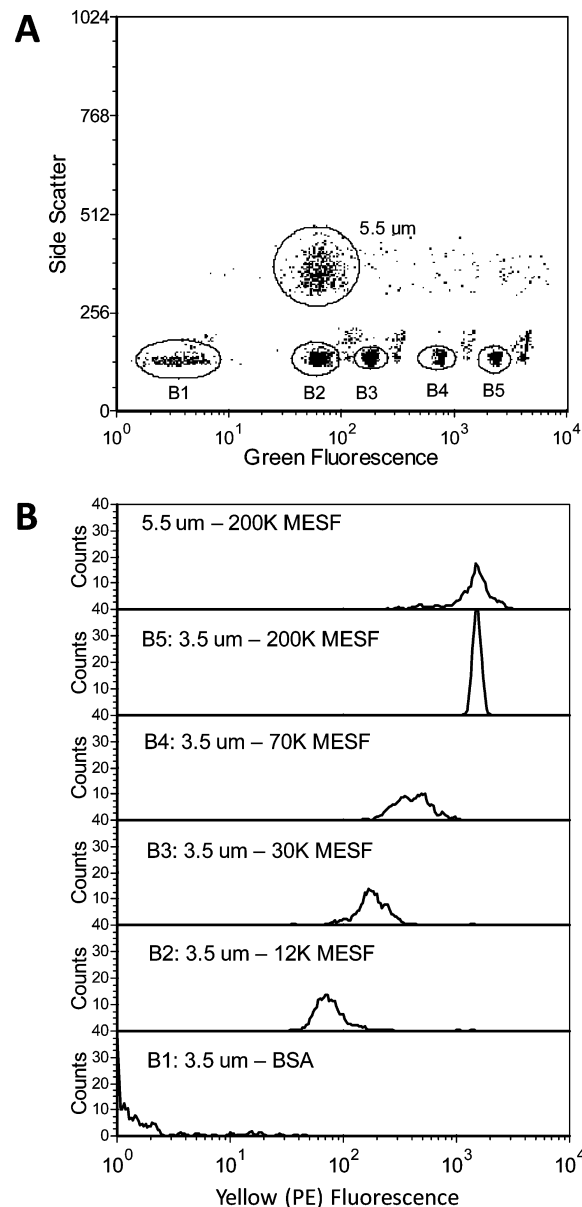


Figure 1. Fluorescence flow cytometry of microspheres with defined binding capacities. A. Bivariate histogram of FALS vs green fluorescence showing populations of fluorescence-encoded 3.5 μm beads (gates B1–B5) and nonfluorescent 5.5 μm beads. B. Yellow fluorescence intensity histograms for the indicated populations of neutravidin-coated beads stained with biotin-PE.

green fluorescence (gates B1–B5), while 5.5 μm beads could be distinguished by their increased light scatter. Gating individual populations in the side scatter vs green fluorescence histogram allows us to measure the fluorescence or SERS from each bead. To determine the bead binding capacity, we stained these beads with a fluorescent ligand, biotinylated phycoerythrin (biotin-PE), and at saturation, and measured them by flow cytometry. After appropriate calibration of the fluorescence signals, we estimated the binding capacity of each bead population (Figure 1B), which ranged from 0 to ~200,000 molecules of biotin-PE.

SERS tags based on gold nanorods are well-established as having a readily tunable plasmon resonance and producing strong SERS from a variety of resonant and nonresonant compounds.^{18–20,23} Given that the use of a resonant compound produces SERS signals that are significantly stronger compared

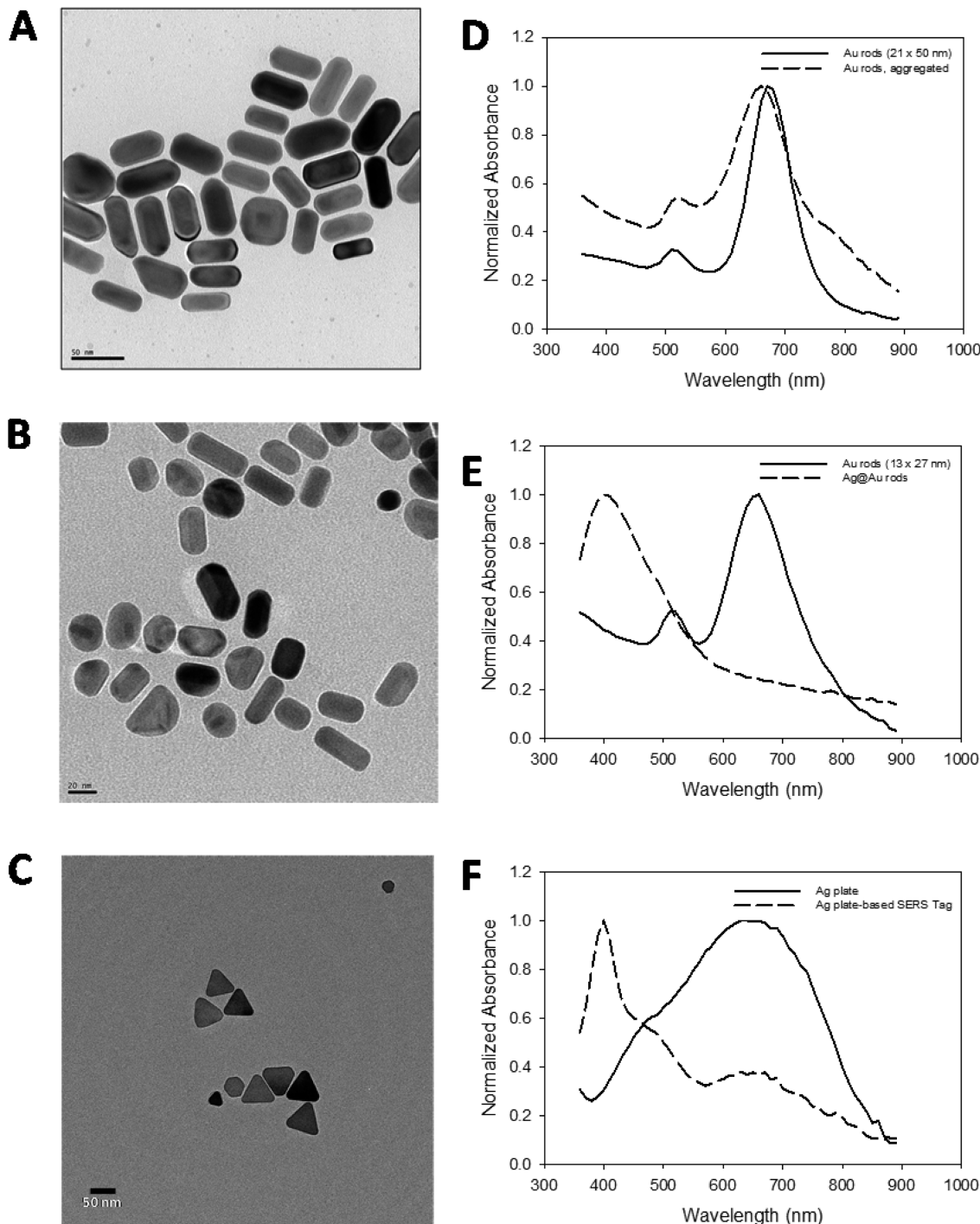


Figure 2. Characterization of the plasmonic particles used to prepare SERS tags in this study. A–C. TEM images of large Au nanorods (A, scale bar: 50 nm), Ag@Au nanorods (B, scale bar: 20 nm), and Ag plates (C, scale bar: 50 nm). D. UV/vis extinction spectra of monodisperse (solid line) and aggregated Au rods (dashed line). E. UV/vis extinction spectra of Au rods (solid line) and Ag@Au rods (dashed line). F. UV/vis extinction spectra of Ag plates (solid line) and Ag plate-based SERS tags (dashed line).

to nonresonant compounds,^{3,45} we focused on MGITC, a Raman tag that binds strongly to Au and Ag nanoparticles, absorbs near our excitation and nanoparticle resonance wavelength, and produces strong SERS from a variety of nanoparticle types. We stained the calibrated neutravidin microspheres with red-excited Au nanorod SERS tags (Figure 2A) and measured the resulting SERS intensity on a custom spectral flow cytometer using excitation at 488 to measure the green fluorescence from the microsphere encoding dye and

excitation at 660 nm to measure the entire microsphere SERS spectra from ~300 to 2000 cm⁻¹ (Figure 3). Presented in Figure 3C are the integrated emission intensity histograms for the different neutravidin density beads. The intensity axis is scaled to photons detected using the detector response calibration provided by the manufacturer. We also used a commercial flow cytometer (FACSCalibur) to excite the SERS tag stained beads at 635 nm and measure the emission between 653 and 669 nm, a band corresponding to a Raman shift of

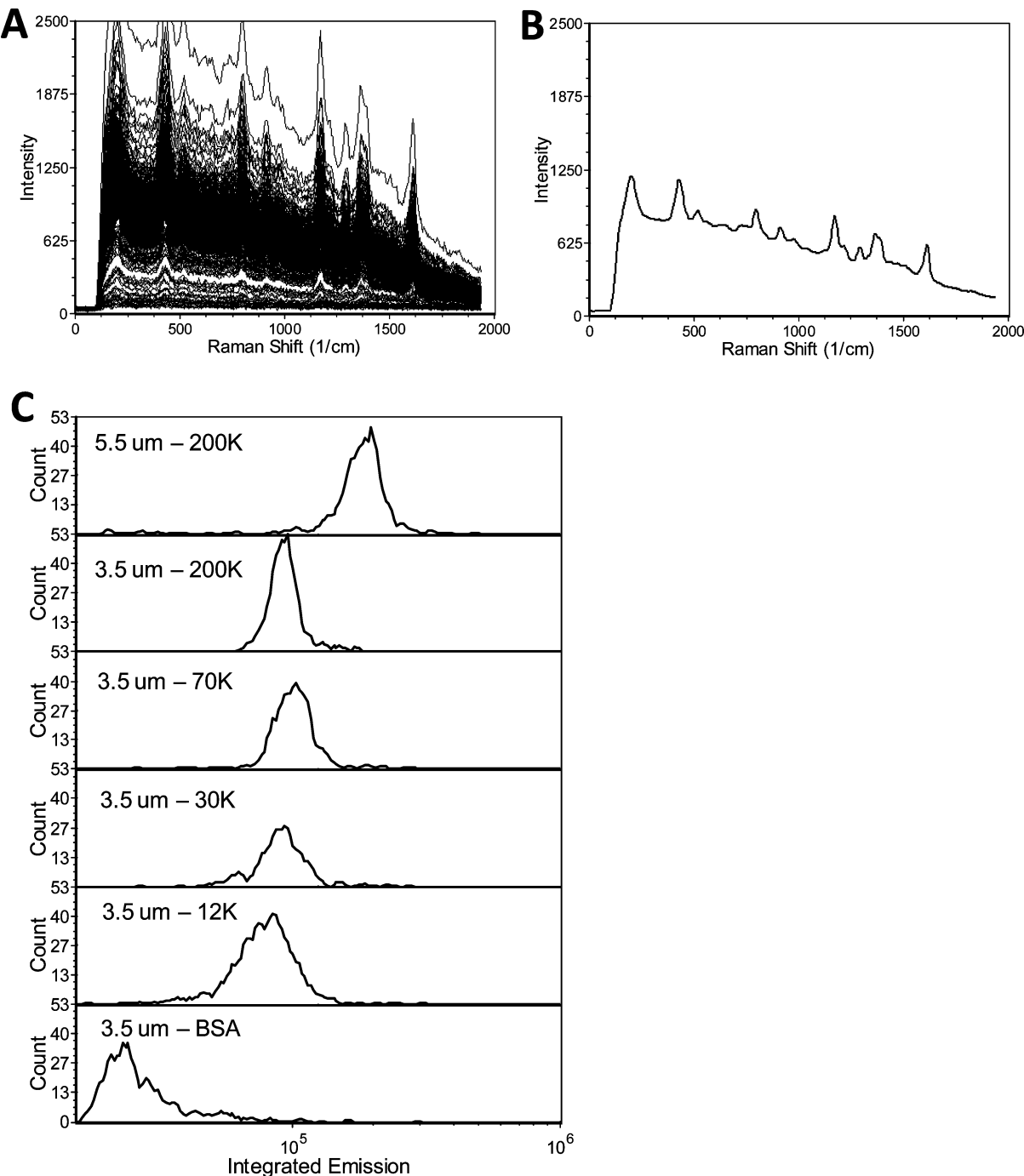


Figure 3. SERS flow cytometry of microspheres stained with biotinylated SERS tags. A. SERS spectra of individual SERS-tag stained beads measured on a spectral flow cytometer. B. Average spectra of SERS tag-stained beads. C. SERS intensity histograms of the neutravidin-density multiplex bead set.

roughly 450–900 cm⁻¹ (Figure 3B), with very similar results (Supporting Information Figure S1). We calibrated the intensity of the low density bead (~12K binding sites) in units of molecules equivalent soluble fluorochrome (MESF) of allophycocyanin (APC), a red-excited fluorophore, using commercially available intensity standard beads and found that the signal from 12,000 Au rod-based SERS tags was equivalent to ~25,000 MESF of APC.

At low binding capacities (0–70,000), the SERS intensity on the 3.5 μm beads increases with increasing binding capacity, and then plateaus at the highest capacity beads (Figure 4A,

filled circles). We interpret this plateau to result from steric hindrance and competition among SERS tags for access to binding sites on the bead surface. We imaged these beads using SEM. Presented in Figure S2 are SEM images of high density avidin beads, showing a high degree of SERS tag surface coverage, low density avidin beads exhibiting subsaturating coverage, and BSA-coated negative control beads, showing a very low amount of nonspecific binding of the biotinylated SERS tags. Upon closer inspection of the SERS tags bound to the neutravidin beads (Figure 5A), it can be seen that the majority of the SERS tags are single rods and dimers (small

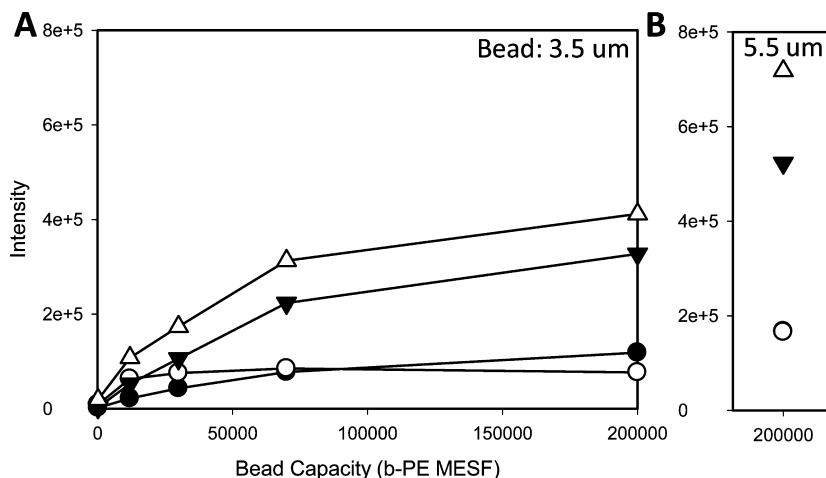


Figure 4. Plots of median SERS intensity versus microsphere binding capacity for 3.5 μm (A) and 5.5 μm (B) neutravidin beads stained with biotinylated SERS tags prepared from four different plasmonic nanoparticles: monodisperse Au rods (filled circles), aggregated Au rods (open circles), Ag@Au rods (solid triangles), and Ag plates (open triangles).

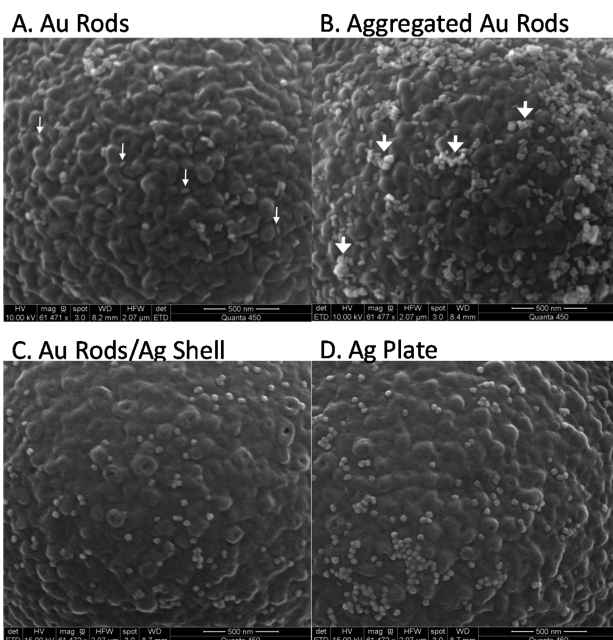


Figure 5. SEM of neutravidin microspheres stained with biotinylated SERS tags. A. Au rod-based SERS tags (small arrows: single nanorods). B. Aggregated Au rod-based SERS tags (large arrows: nanorod aggregates). C. Ag@Au rod-based SERS tags. D. Ag plate-based SERS tags. Magnification: 61,472 \times . Scale bar: 500 nm.

arrows), with relatively few higher order aggregates. Also consistent with the limiting effect of surface density on binding, the larger 5.5 μm beads with a higher capacity but comparable Neutravidin density shows a higher intensity (Figure 4B), reflecting the reduced steric hindrance on the bigger beads. Thus, at low binding site densities, the brightness of a known number of SERS tags can be measured while at higher surface densities the size of the SERS tags limits binding, providing an indication of the effective “footprint” of the SERS tag. For low binding densities (0–12,000 sites), where intensity is expected to be proportional to binding capacity, the slope of this curve reflects the radiant intensity per SERS tag (I_{tag}). At saturation, intensity (I_{sat}) is limited by the physical size of the SERS tag, and the number of SERS tags bound at saturation (N_{sat}) can be

calculated as $I_{\text{sat}}/I_{\text{tag}}$. As the surface area of the microsphere is known, the average cross-sectional footprint of a SERS tag can be calculated, as can the radiant emittance, or size-normalized intensity, of each SERS tag. The radiant emittance is arguably the most important determinant of a SERS tag’s assay performance, and thus is of prime interest in comparing different SERS tags. We applied this approach to several different SERS tag compositions based on different plasmonic nanoparticles, but with the same Raman active compound, MGITC, and the same coating of biotin-functionalized PEG.

First, we evaluated SERS tags based on red-resonant Au nanorods exhibiting different levels of aggregation. The aggregation of plasmonic particles can induce a shift in the localized surface plasmon resonance and generate “hotspots” of high local E field intensity, making aggregation a popular way to increase SERS intensity. When Au nanorod-based SERS tags are prepared as we have described previously,³⁵ the degree of aggregation, as evidenced by a red-shift in the extinction spectrum (Figure 2D), can be affected by the acid washing step used to remove CTAB from the rod surface. Using a single stock of CTAB-stabilized red-resonant Au nanorods (approximately $25 \times 50 \text{ nm}^2$), we prepared two lots of MGITC biotinylated SERS tags exhibiting different degrees of aggregation, as judged from the red-shifted shoulder in the UV-vis extinction spectrum (Figure 1D). We used these to stain the calibrated bead set described above and measured them using spectral flow cytometry. Inspection of SEM images of these SERS tags bound to neutravidin beads (Figure 5B) reveals a heterogeneous population of large aggregates (large arrows), with relatively fewer monomers and dimers seen with unaggregated tags. This qualitative assessment is confirmed by NTA measurement, which also indicates significantly larger SERS tags when compared to those prepared from unaggregated rods (Table 1, SI Figure S3A). Plots of intensity vs binding capacity (Figure 4, open circles) show saturation at lower binding densities compared to unaggregated rods. Analysis of these data as above (Table 1) shows that the intensity of tags prepared with aggregated rods (Tags B.1 and B.2) is approximately 2–4 times higher than tags prepared from less aggregated rods (Tag A.1), while the binding footprint is approximately 1.5 times larger. When the size-normalized intensity is considered, the aggregated Au rod-based tags have a

Table 1. Characterization of the SERS Tags Used in the Study

tag	base particle description	size, TEM (nm)	I_{tag} (pe ⁻)	# tags/3.5 um bead	footprint (nm ²)	emittance (pe ⁻ /nm ² ×1000)	SERS tag diameter, NTA (nm)
A.1	Au rod	54 × 23	2.91	65,548	587	4.95	49
B.1	Au rod (aggregated)	50 × 21	8.48	14,583	2640	3.21	113
B.2	Au rod (aggregated)	50 × 21	4.36	18,668	2062	2.11	103
C.1	Ag@Au rod	27 × 13	10.21	47,714	807	12.66	62
C.2	Ag@Au rod	27 × 13	7.05	74,694	515	13.68	73
C.3	Ag@Au rod	nd ^a	4.08	89,888	428	9.52	59
C.4	Ag@Au rod	40 × 20	4.83	58,453	659	7.33	73
D.1	Ag plate	nd	8.96	45,923	838	10.69	108
D.2	Ag plate	nd	7.82	39,985	963	8.13	106
D.3	Ag plate	nd	9.13	41,958	918	9.95	89

^and, not determined.

lower radiant emittance than SERS tags made from monodisperse Au rods.

Next, we prepared MGITC SERS tags based on a Ag shell over a Au rod (Ag@Au rod). We prepared red resonant Au nanorods (~10 × 25 nm) and coated them with Ag. These Au rods were smaller than those used above and, as prepared, produced fairly dim SERS signals with MGITC (data not presented), but after Ag coating the resulting plasmonic base particles produced significantly brighter SERS tags that are comparable in size to the larger unaggregated Au rods described above. We used these bimetallic core–shell-based SERS tags to stain the calibrated bead set (Figure 4, filled triangles), and analyzed the results as above. We found that the per tag intensity of these Ag@Au rod-based SERS tags was comparable to that of SERS tags made from aggregated Au rods, but that the binding footprint was more similar to SERS tags made from monodisperse Au rods, resulting in tags that are ~3–5 times brighter on a size-normalized basis than either rod-based tag. Inspection of these SERS tags bound to beads show primarily monodisperse particles without much evidence of aggregation, consistent with NTA diameter estimates (Tags C.1–4, Table 1; Figure 5; SI Figure S3B).

Finally, we prepared MGITC SERS tags based on Ag plates. Red resonant plates were incubated with an optimal amount of MGITC, followed by sulphydryl PEG-biotin, and washed. We stained calibrated capture beads with these SERS tags (Figure 4, open triangles) and analyzed the results as above. The Ag plate-based SERS tags (Tags D.1–3) had single tag intensities and radiant emittance comparable to the Au rod/Ag shell-based tags (Table 1). Inspection of SEM images of capture beads with Ag plate-based SERS tags (Figure 5D) reveals mostly monodisperse particles (~50 nm diameter), consistent with NTA diameter estimates (Table 1; SI Figure S3C).

To evaluate how the bright tags performed in cell analysis applications, we conjugated antibodies to Au rod-, Ag@au rod-, and Ag plate-based SERS tags (similar to those above, but bearing carboxy groups instead of biotin) and used these to stain cells for analysis by spectral flow cytometry. We cultured two breast cancer cell lines: BT474, which expresses high levels of the cell surface receptor HER2, and MDA-MB-435, which does not. These cells were fixed and stained with an anti-HER2 primary antibody, followed by an anti-mouse IgG conjugated SERS tag secondary label. Presented in Figure 6 are average single cell spectra from these cells, as well as spectra from secondary-only and unstained cells. The Au rod-based SERS tags allowed resolution of HER2 positive and negative cell lines, but with only ~10-fold difference in the median intensities of

the cell populations. As expected from the calibration results summarized in Table 1, cells stained with SERS tags based on Ag@Au rod cores and Ag plates showed brighter staining and better resolution from unstained and secondary-only stained cells, with the Ag plate-based tags producing a >100-fold separation of the population mean intensities. This performance advantage, combined with the relative ease of preparing Ag plate-based SERS tags compared to rod-based SERS tags, makes these tags attractive for cell analysis and other applications.

In summary, we present a general approach to characterize the brightness and staining performance of nanoparticle SERS tags in the context of a surface binding assay. By measuring the binding of SERS tags to microspheres with different densities of binding sites, we are able to estimate the relative single tag brightness and binding footprint of several different SERS tag compositions. We show that the SERS radiant emittance is a good predictor of performance in flow cytometry analysis of mammalian cells, and that this approach should be generalizable to other applications and assay platforms as well. The analysis we present can be performed using widely available reagents and commercial flow cytometers and represents a straightforward approach to interlab standardization of SERS tag intensity and assay performance.

MATERIALS AND METHODS

Reagents. Fluorescent and nonfluorescent carboxylated microspheres were from Spherotech. 1-Ethyl-3-[3-(dimethylamino)propyl]carbodiimide hydrochloride (EDC), N-hydroxysuccinimide (NHS), and Neutravidin were from Thermo. Malachite Green isothiocyanate (MGITC), biotinylated phycoerythrin (b-PE), and Linear Flow Deep Red beads were from Life Technologies. Quantum MESF APC beads were from Bangs Laboratory. Mouse anti-human HER2 (clone 24D2) was from Biolegend and goat anti-mouse IgG (H+L) antibody was from Protein Biosystems. BSA and all other reagents were from Sigma-Aldrich unless otherwise indicated.

Preparation and Characterization of Microspheres with Defined Binding Capacity. Carboxylated beads (5×10^7 /mL) were incubated with a mixture of Neutravidin and BSA in varying ratios (0:10, 1.5:8.5; 2.5:7.5, 4:6; 10:0; 10 μ g total protein per 100 μ L reaction) for 15 min, followed by addition of EDC (5 mg/mL) and NHS (5 mg/mL) and incubation for 60 min with occasional mixing. Beads were then diluted in PBS/Tween 20 (0.05%) and washed twice by centrifugation and resuspension, and stored in the same buffer. To measure binding capacity, beads were stained with

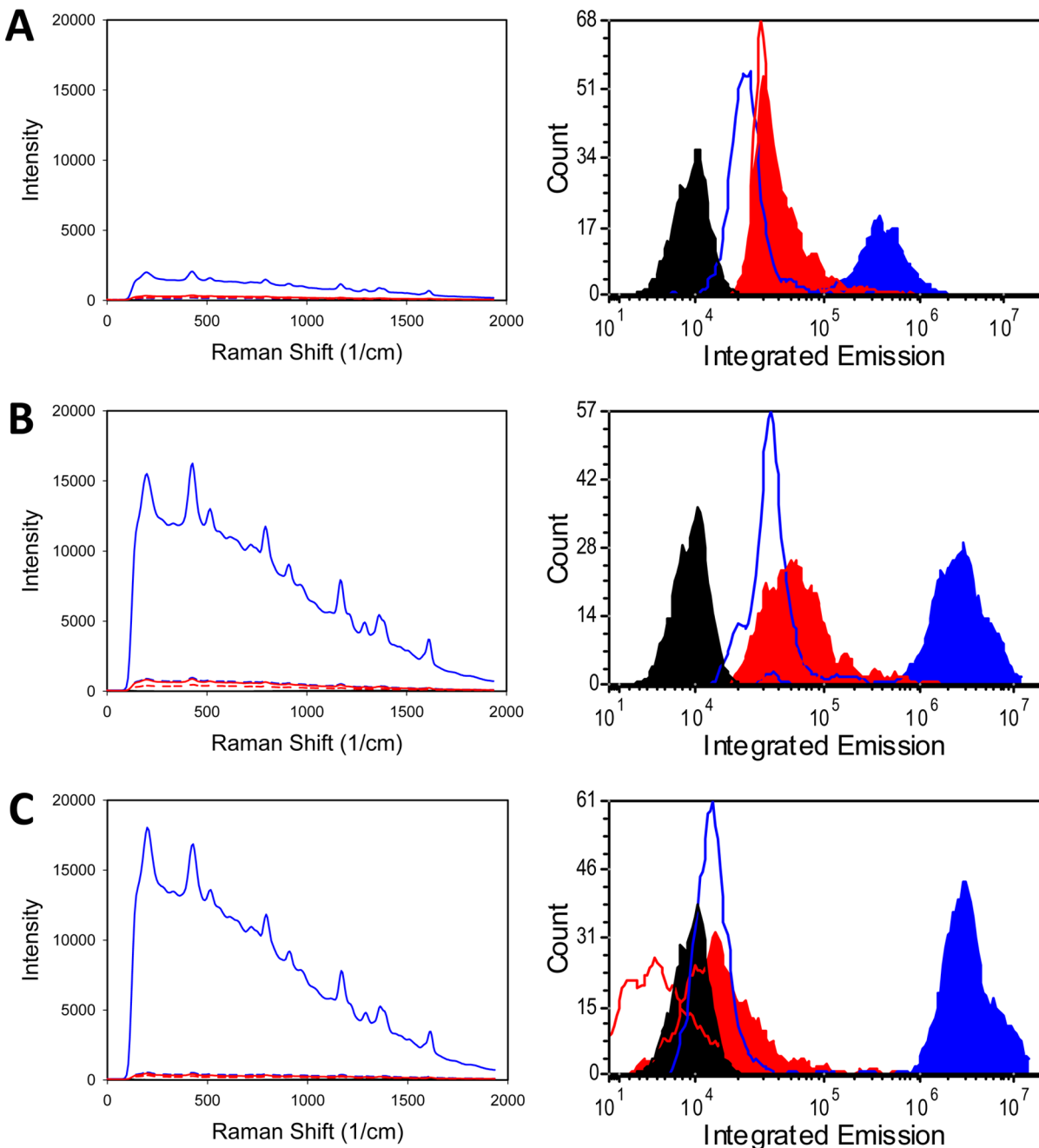


Figure 6. Performance of SERS tags in spectral flow cytometry. Breast cancer cell lines BT474 (HER2+) and MB435 (HER2-) were stained with anti-HER2 conjugated primary antibody followed by anti-mouse IgG SERS tags prepared from (A) gold nanorods, (B) Ag@Au nanorods, and (C) Ag plates. Left column: Average spectra from unstained cells (black), BT474 (blue), and MB435 (red), with (solid line) or without (dotted line) primary antibody. Right column: Intensity histograms from unstained cells (black), BT474 (blue), and MB 435 (red), with (solid fill) or without (no fill) primary antibody.

biotinylated PE at saturating concentration (50 nM) in PBST, and their fluorescence measured by flow cytometry (FACSCalibur, BD Biosciences). Forward angle and 90° light scatter (488 nm), green (488 nm excitation, 530 ± 30 nm emission), and yellow fluorescence (488 nm excitation, 585 ± 42 nm emission) of at least 1000 individual beads were measured. The intensity of the yellow fluorescence was calibrated in units of molecules of equivalent soluble fluorophores (MESF) of PE by measuring calibrated standard beads (QuantiBrite PE, BD Biosciences) at the same detector setting.

Plasmonic Nanoparticles. Au nanorods were prepared based on modifications of published protocols, as described

previously.^{22,46} Briefly, for large rods³⁵ (20×50 nm²; Figure 1A), gold seed was prepared by adding 5 mL of a 0.0005 M HAuCl₄ solution to 5 mL of an aqueous hexadecyltrimethylammonium bromide (CTAB) solution (0.2 M). To the vigorously stirred solution, 0.21 mL of 0.026 M ice cold NaBH₄ is added to produce a light-brown solution. Stirring was continued for 2 more minutes, after which the seed solution was kept in a water bath at 25 °C for up to 2 h. Then, 500 mL of a 0.2 M aqueous CTAB solution was mixed with 0.1 mL AgNO₃ at 0.004 M followed by addition of 500 mL of 0.001 M HAuCl₄ to form the growth solution. After vigorous mixing, 7 mL of 0.0788 M L-ascorbic acid was added, and the solution

incubated in a 25 °C water bath. After 10 min, the solution was removed from the water bath, 1.2 mL of the seed solution added, and the mixture stirred for 2 min. The solution was then placed back in the 25 °C water bath for 18 h. After fabrication, excess CTAB was removed by incubating rods at 4 °C overnight and then removing supernatant and discarding precipitated CTAB.

To produce Ag@Au rods (Figure 1B), smaller Au rods ($10 \times 25 \text{ nm}^2$) were prepared as described.⁴⁶ Briefly, 666 mL of a 0.2 M aqueous CTAB solution was gently swirled with 333 mL HAuCl₄ and warmed to 27 °C. Then 5 mL of 0.004 M AgNO₃ was added and the solution was gently swirled. Then 1.27 mL of 5 M HCl was added without mixing, followed by addition of 4.6 mL of 0.078 M ascorbic acid. Solution was gently swirled until color changed from yellow to clear and then 1 mL of 0.01 M NaBH₄ was added without mixing. The solution was then placed back in the 25 °C water bath undisturbed for 18 h. After fabrication, excess CTAB was removed by incubating rods at 4 °C overnight and then removing supernatant and discarding precipitated CTAB. These Au rods were then coated with a shell of Ag. First, nanorods were washed by centrifugation into nanopure water. Then, with magnetic stirring, 300 μL/mL of 0.1 M AgNO₃ was added, followed immediately by 300 μL/mL of 37% formaldehyde and 30 μL/mL 0.83 M NH₄OH. Formation of the Ag shell resulted in a blue shift of the extinction spectrum (Figure 1E).

Ag plates (Figure 1C) were prepared as described by Zhang,⁴⁷ 0.05 mL of 0.05 M AgNO₃ was added to 24.75 mL of nanopure water with gentle stirring. To this solution, 0.5 mL of 0.075 M trisodium citrate, 0.1 mL of 17.5 M glycerol, 0.06 mL of 30% H₂O₂, and 0.25 mL of 0.1 M NaBH₄ were added. Reaction was complete after 5 min when color changed from clear to dark blue. Ag plates were washed by centrifugation to remove excess capping agent before use. The Ag plates have a broad extinction spectra with a peak in the red (~670 nm, Figure 1F).

SERS Tag Preparation. To prepare SERS tags, large nanorods were incubated with 32 μM HCl at 60 °C for 45 min to remove CTAB, and then washed twice. This step of the protocol results in a degree of aggregation of the nanorods, as evidenced by a red shift in the UV/vis extinction spectrum (Figure 1D), that can vary between preparations. Ag-coated Au nanorods and Ag plates were used as prepared. Raman tag (MGITC) at an optimal concentration (determined beforehand via titration and generally in the range of 0.1 to 1 μM) was incubated with the plasmonic base particle for 15 min at ambient temperature. Functionalized sulphydral PEG (0.5 μM, carboxylated or biotinylated, 3000 MW, Rapp Polymer) and 5 μM unfunctionalized sulphydral PEG (CH₃, 2000 MW, Nanocs) was then added and incubated with the tagged nanorods for 15 min at ambient temperature, and then overnight at 4 °C. The SERS tags were then washed by three cycles of centrifugation and resuspension and characterized by UV/vis and Raman spectroscopy. The extinction spectra of the Au rods and Ag shell/Au rods did not change during preparation of the SERS tags. However, the Ag plate-based SERS tag exhibited a blue-shifted extinction spectrum (Figure 1F), suggesting a change in nanoparticle structure associated with binding of the MGITC and sulphydral PEG ligands. Goat anti-mouse antibody was coupled to carboxylated SERS tags as described.³⁵

SERS Tag Binding and Measurement. SERS tags (0.5–2 nM particles) were incubated with 10 μL of beads or cells (5 × 10⁷/mL) in 100 μL for 2 h at ambient temperature in a

microwell plate with shaking. The concentration of each SERS tag needed to reach binding saturation was determined in preliminary titrations. After incubation, samples were washed 3× with PBST using a filter plate (1.2 μm pore size, Millipore) vacuum apparatus. The SERS tag was measured using a commercial flow cytometer as described above or with a custom spectral flow cytometer. For conventional flow cytometry (BD Biosciences FACSCalibur), SERS was excited at 635 nm and emission measured through a 661 ± 16 nm bandpass filter. The SERS intensity was calibrated in units of MESF of APC, a red-excited fluorophore, using fluorescent hard-dyed beads (Linear Flow Deep Red) that had been cross calibrated against APC standard beads (Quantum MESF) on that instrument. SERS tag binding was also measured on a custom spectral flow cytometer^{35,44,48} using spatially separated laser spots at 488 and 660 nm. Forward angle light scatter, 90° light scatter, and green fluorescence (525 ± 20 nm emission) excited by 488 nm were measured as for conventional fluorescence flow cytometry. SERS was excited at 660 nm and collected light was dispersed by an imaging spectrograph (Kaiser, Holospec) with a 660 nm edge filter (Razor Edge, Semrock) through a volume phase holographic grating onto an EM-CCD (Newton 970U-BV, Andor). Spectra from individual beads were collected and the integrated intensity calculated for each.

Nanoparticle Tracking Analysis (NTA) of SERS Tags.

The hydrodynamic radius of SERS tag was estimated using a nanoparticle tracking analyzer (LM-20, Nanosight) equipped with a 532 nm laser and high sensitivity CMOS camera. Samples were diluted in 0.1 μm filtered H₂O, loaded into the analysis chamber and three videos of 30 s each were acquired for each sample. The Brownian diffusion of >200 individual particles was analyzed and the hydrodynamic radius for each estimated using the NanoSight software.

Electron Microscopy. Transmission electron microscopy was performed on samples deposited onto carbon grids (EM Sciences) and dried. Grids were imaged on a FEI Tecnai Sphera at the University of California San Diego Cryo-EM facility or at the National Resource for Automated Microscopy at the Scripps Research Institute. Particle dimensions were estimated using a semiautomated ImageJ script. For scanning EM, samples were deposited on nucleopore polycarbonate membrane filters (Millipore, average pore diameter 200 nm), mounted on sample stubs and coated under vacuum with a 5 nm layer of platinum. Samples were imaged with a FEI Quanta 450 FEG Scanning Electron Microscope at the San Diego State University Electron Microscopy facility.

ASSOCIATED CONTENT

Supporting Information

Conventional flow cytometry measurements, SEM images, and nanoparticle tracking data. This material is available free of charge via the Internet at <http://pubs.acs.org>.

AUTHOR INFORMATION

Corresponding Author

*E-mail: jnolan@scintillon.org.

Present Address

[†]John P. Nolan: The Scintillon Institute, 6404 Nancy Ridge Drive, San Diego, California 92121.

Notes

The authors declare no competing financial interest.

ACKNOWLEDGMENTS

We thank Samuel Stoner (University of California San Diego) and Tilak Jain (The Scripps Research Institute) for producing the TEM images, Steve Barlow (San Diego State University) for producing the SEM images, and Er Liu (LJBI) for culture of the breast cancer cell lines. Some of the work presented here was conducted at the National Resource for Automated Molecular Microscopy which is supported by a grant from the National Institute of General Medical Sciences (9 P41 GM103310) from the National Institutes of Health. Supported by a Bioengineering Research Partnership grant (R01 EB003824) from the National Institute of Bioimaging and Bioengineering of the National Institutes of Health.

REFERENCES

- (1) Jeanmaire, D. L., and Van Duyne, R. P. (1977) Surface raman spectroelectrochemistry: Part I. Heterocyclic, aromatic, and aliphatic amines adsorbed on the anodized silver electrode. *J. Electroanal. Chem. Interfacial Electrochem.* 84, 1–20.
- (2) Moskovits, M. (1985) Surface-enhanced spectroscopy. *Rev. Mod. Phys.* 57, 783–826.
- (3) Nie, S., and Emory, S. R. (1997) Probing single molecules and single nanoparticles by surface-enhanced raman scattering. *Science* 275, 1102–1106.
- (4) Alvarez-Puebla, R. A., and Liz-Marzán, L. M. (2010) SERS-based diagnosis and biodetection. *Small* 6, 604–610.
- (5) Porter, M. D., Lipert, R. J., Siperko, L. M., Wang, G., and Narayanan, R. (2008) SERS as a bioassay platform: fundamentals, design, and applications. *Chem. Soc. Rev.* 37, 1001–1011.
- (6) Schlücker, S. (2009) SERS microscopy: nanoparticle probes and biomedical applications. *ChemPhysChem* 10, 1344–1354.
- (7) Doering, W. E., Piotti, M. E., Natan, M. J., and Freeman, R. G. (2007) SERS as a foundation for nanoscale, optically detected biological labels. *Adv. Mater.* 19, 3100–3108.
- (8) Mulvaney, S. P., Musick, M. D., Keating, C. D., and Natan, M. J. (2003) Glass-coated, analyte-tagged nanoparticles: a new tagging system based on detection with surface-enhanced Raman scattering. *Langmuir* 19, 4784–4790.
- (9) Doering, W. E., and Nie, S. (2003) Spectroscopic tags using dye-embedded nanoparticles and surface-enhanced Raman scattering. *Anal. Chem.* 75, 6171–6176.
- (10) Kleinman, S. L., Sharma, B., Blaber, M. G., Henry, A.-I., Valley, N., Freeman, R. G., Natan, M. J., Schatz, G. C., and Van Duyne, R. P. (2012) Structure enhancement factor relationships in single gold nanoantennas by surface-enhanced Raman excitation spectroscopy. *J. Am. Chem. Soc.* 135, 301–308.
- (11) McMahon, J. M., Henry, A.-I., Wustholz, K. L., Natan, M. J., Freeman, R. G., Van Duyne, R. P., and Schatz, G. C. (2009) Gold nanoparticle dimer plasmonics: finite element method calculations of the electromagnetic enhancement to surface-enhanced Raman spectroscopy. *Anal. Bioanal. Chem.* 394, 1819–1825.
- (12) Wustholz, K. L., Henry, A.-I., McMahon, J. M., Freeman, R. G., Valley, N., Piotti, M. E., Natan, M. J., Schatz, G. C., and Duyne, R. P. V. (2010) Structure–activity relationships in gold nanoparticle dimers and trimers for surface-enhanced Raman spectroscopy. *J. Am. Chem. Soc.* 132, 10903–10910.
- (13) Sha, M. Y., Xu, H., Natan, M. J., and Cromer, R. (2008) Surface-enhanced Raman scattering tags for rapid and homogeneous detection of circulating tumor cells in the presence of human whole blood. *J. Am. Chem. Soc.* 130, 17214–5.
- (14) Zavaleta, C., De La Zerda, A., Liu, Z., Keren, S., Cheng, Z., Schipper, M., Chen, X., Dai, H., and Gambhir, S. (2008) Noninvasive Raman spectroscopy in living mice for evaluation of tumor targeting with carbon nanotubes. *Nano Lett.* 8, 2800–2805.
- (15) Jokerst, J. V., Miao, Z., Zavaleta, C., Cheng, Z., and Gambhir, S. S. (2011) Affibody-functionalized gold–silica nanoparticles for Raman molecular imaging of the epidermal growth factor receptor. *Small* 7, 625–633.
- (16) Grzelczak, M., Pérez-Juste, J., Mulvaney, P., and Liz-Marzán, L. M. (2008) Shape control in gold nanoparticle synthesis. *Chem. Soc. Rev.* 37, 1783–1791.
- (17) Jain, P. K., Huang, X., El-Sayed, I. H., and El-Sayed, M. A. (2008) Noble metals on the nanoscale: optical and photothermal properties and some applications in imaging, sensing, biology, and medicine. *Acc. Chem. Res.* 41, 1578–1586.
- (18) Murphy, C. J., Sau, T. K., Gole, A. M., Orendorff, C. J., Gao, J., Gou, L., Hunyadi, S. E., and Li, T. (2005) Anisotropic metal nanoparticles: synthesis, assembly, and optical applications. *J. Phys. Chem. B* 109, 13857–13870.
- (19) Nikoobakht, B., and El-Sayed, M. A. (2003) Preparation and growth mechanism of gold nanorods (NRs) using seed-mediated growth method. *Chem. Mater.* 15, 1957–1962.
- (20) Perez-Juste, J., Pastoriza-Santos, I., Liz-Marzán, L. M., and Mulvaney, P. (2005) Gold nanorods: synthesis, characterization and applications. *Coord. Chem. Rev.* 249, 1870–1901.
- (21) Sau, T. K., and Murphy, C. J. (2004) Seeded high yield synthesis of short Au nanorods in aqueous solution. *Langmuir* 20, 6414–6420.
- (22) Nolan, J. P., and Sebba, D. S. (2011) Surface-Enhanced Raman Scattering (SERS) Cytometry, in *Methods in Cell Biology* (Paul, M., Ed.) pp 515–532, Academic Press.
- (23) von Maltzahn, G., Centrone, A., Park, J. H., Ramanathan, R., Sailor, M. J., Hatton, T. A., and Bhatia, S. N. (2009) SERS coded gold nanorods as a multifunctional platform for densely multiplexed near infrared imaging and photothermal heating. *Adv. Mater.* 21, 3175–3180.
- (24) Sebba, D. S., Watson, D. A., and Nolan, J. P. (2009) High throughput single nanoparticle spectroscopy. *ACS Nano* 3, 1477–1484.
- (25) Wu, L., Wang, Z., Zong, S., Huang, Z., Zhang, P., and Cui, Y. (2012) A SERS-based immunoassay with highly increased sensitivity using gold/silver core-shell nanorods. *Biosens. Bioelectron.* 38, 94–95.
- (26) Xu, S., Ji, X., Xu, W., Zhao, B., Dou, X., Bai, Y., and Ozaki, Y. (2005) Surface-enhanced Raman scattering studies on immunoassay. *J. Biomed. Opt.* 10, 031112–031112–12.
- (27) Zong, S., Wang, Z., Yang, J., Wang, C., Xu, S., and Cui, Y. (2012) A SERS and fluorescence dual mode cancer cell targeting probe based on silica coated Au@ Ag core–shell nanorods. *Talanta* 97, 368–375.
- (28) Abalde-Cela, S., Aldeanueva-Potel, P., Mateo-Mateo, C., Rodríguez-Lorenzo, L., Alvarez-Puebla, R. A., and Liz-Marzán, L. M. (2010) Surface-enhanced Raman scattering biomedical applications of plasmonic colloidal particles. *J. R. Soc. Interface* 7, S435.
- (29) Alvarez Puebla, R. A., and Liz Marzán, L. M. (2010) SERS based diagnosis and biodetection. *Small* 6, 604–610.
- (30) Chon, H., Lim, C., Ha, S. M., Ahn, Y., Lee, E. K., Chang, S. I., Seong, G. H., and Choo, J. (2010) On-chip immunoassay using surface-enhanced Raman scattering of hollow gold nanospheres. *Anal. Chem.* 82, 5290–5295.
- (31) Cui, Y., Ren, B., Yao, J. L., Gu, R. A., and Tian, Z. Q. (2007) Multianalyte immunoassay based on surface-enhanced Raman spectroscopy. *J. Raman Spectrosc.* 38, 896–902.
- (32) Kennedy, D. C., Hoop, K. A., Tay, L. L., and Pezacki, J. P. (2010) Development of nanoparticle probes for multiplex SERS imaging of cell surface proteins. *Nanoscale* 2, 1413–1416.
- (33) McNay, G., Eustace, D., Smith, W. E., Faulds, K., and Graham, D. (2011) Surface-enhanced raman scattering (SERS) and surface-enhanced resonance Raman scattering (SERRS): a review of applications. *Appl. Spectrosc.* 65, 825–837.
- (34) Neng, J., Harpster, M. H., Zhang, H., Mecham, J. O., Wilson, W. C., and Johnson, P. A. (2010) A versatile SERS-based immunoassay for immunoglobulin detection using antigen-coated gold nanoparticles and malachite green-conjugated protein A/G. *Biosens. Bioelectron.* 26, 1009–1015.

- (35) Nolan, J. P., Duggan, E., Liu, E., Condello, D., Dave, I., and Stoner, S. A. (2012) Single cell analysis using surface enhanced Raman scattering (SERS) tags. *Methods* 57, 272–9.
- (36) Hoffman, R. A., and Wood, J. C. S. (2007) Characterization of Flow Cytometer Instrument Sensitivity, in *Current Protocols in Cytometry*, John Wiley & Sons, Inc.
- (37) Schwartz, A., Fernandez Repollet, E., Vogt, R., and Gratama, J. W. (1996) Standardizing flow cytometry: construction of a standardized fluorescence calibration plot using matching spectral calibrators. *Cytometry* 26, 22–31.
- (38) Schwartz, A., Gaigalas, A. K., Wang, L., Marti, G. E., Vogt, R. F., and Fernandez-Repollet, E. (2004) Formalization of the MESF unit of fluorescence intensity. *Cytometry, Part B* 57, 1–6.
- (39) Schwartz, A., Wang, L., Early, E., Gaigalas, A., Zhang, Y.-z., Marti, G. E., and Vogt, R. F. (2002) Quantitating fluorescence intensity from fluorophore: The definition of MESF assignment. *J. Res. Natl. Inst. Stand. Technol.* 107, 83–92.
- (40) Woods, T. A., Graves, S. W., and Nolan, J. P. (2005) Microsphere surface protein determination using flow cytometry. *Current Protocols in Cytometry*, 13.2. 1–13.2. 13.
- (41) Keeney, M., Chin-Yee, I., Weir, K., Popma, J., Nayar, R., and Sutherland, D. R. (1998) Single platform flow cytometric absolute CD34+ cell counts based on the ISHAGE guidelines. *Cytometry* 34, 61–70.
- (42) Graves, S. W., Woods, T. A., Kim, H., and Nolan, J. P. (2005) Direct fluorescent staining and analysis of proteins on microspheres using CBQCA. *Cytometry, Part A* 65, 50–58.
- (43) Mittal, R., and Bruchez, M. P. (2009) Calibration of flow cytometry for quantitative quantum dot measurements. *Current Protocols in Cytometry*, 6.26. 1–6.26. 7.
- (44) Nolan, J. P., Condello, D., Duggan, E., Naivar, M., and Novo, D. (2012) Visible and near infrared fluorescence spectral flow cytometry. *Cytometry, Part A* 83, 253–264.
- (45) Kneipp, K., Wang, Y., Kneipp, H., Perelman, L. T., Itzkan, I., Dasari, R. R., and Feld, M. S. (1997) Single molecule detection using surface-enhanced Raman scattering (SERS). *Phys. Rev. Lett.* 78, 1667–1670.
- (46) Ali, M. R. K., Snyder, B., and El-Sayed, M. A. (2012) Synthesis and optical properties of small Au nanorods using a seedless growth technique. *Langmuir* 28, 9807–9815.
- (47) Zhang, Q., Li, N., Goebel, J., Lu, Z., and Yin, Y. (2011) A systematic study of the synthesis of silver nanoplates: is citrate a “magic” reagent? *J. Am. Chem. Soc.* 133, 18931–18939.
- (48) Watson, D. A., Brown, L. O., Gaskill, D. F., Naivar, M., Graves, S. W., Doorn, S. K., and Nolan, J. P. (2008) A flow cytometer for the measurement of Raman spectra. *Cytometry, Part A* 73, 119–128.